

# Topological insulator materials for advanced optoelectronic devices

Zengji Yue<sup>1</sup>, Xiaolin Wang<sup>1</sup> and Min Gu<sup>2</sup>

<sup>1</sup>*Institute for Superconducting & Electronic Materials, University of Wollongong, North Wollongong, New South Wales 2500, Australia*

<sup>2</sup>*Laboratory of Artificial-Intelligence Nanophotonics, School of Science, RMIT University, Melbourne, Victoria 3001, Australia*

Email: [zengji@uow.edu.au](mailto:zengji@uow.edu.au)

## Abstract

Topological insulators are quantum materials that have an insulating bulk state and a topologically protected metallic surface state with spin and momentum helical locking and a Dirac-like band structure.[1-3] Two-dimensional (2D) topological insulators are associated with gapless edge states, and three-dimensional (3D) topological insulators with gapless surface states.[4] A variety of compounds have been identified as 2D or 3D topological insulators, including HgTe/CdTe, Bi<sub>2</sub>Se<sub>3</sub>, Bi<sub>2</sub>Te<sub>3</sub>, Sb<sub>2</sub>Te<sub>3</sub>, BiTeCl, Bi<sub>1.5</sub>Sb<sub>0.5</sub>Te<sub>1.8</sub>Se<sub>1.2</sub>, SmB<sub>6</sub>, and others.[5-8] The topological surface (edge) states in these materials have been mainly investigated by first-principles theoretical calculations, electronic transport measurements, angle-resolved photoemission spectroscopy, and scanning tunneling microscopy.[6] Unique and fascinating electronic properties, such as the quantum spin Hall effect, quantum anomalous Hall effect, and topological magnetoelectric effect, as well as magnetic monopole images and Majorana fermions, have been observed in the topological insulator materials.[9, 10] With these unique properties, topological insulator materials have great potential applications in spintronics and quantum information processing, as well as magnetoelectric devices with higher efficiency and lower energy consumption.[11, 12]

On the other hand, topological insulator materials also exhibit a number of excellent optical properties, including Kerr and Faraday rotation, ultrahigh bulk refractive index, near-infrared frequency transparency, unusual electromagnetic scattering, and ultra-broadband surface plasmon resonances.<sup>[13]</sup> Specifically, Dirac plasmon excitations have been observed in Bi<sub>2</sub>Se<sub>3</sub> micro-ribbon arrays at THz frequencies.[14] Ultraviolet and visible frequency plasmonics

have been observed in nanoslit and nanocone arrays of  $\text{Bi}_{1.5}\text{Sb}_{0.5}\text{Te}_{1.8}\text{Se}_{1.2}$  crystals.[15, 16] High transparency has been observed in  $\text{Bi}_2\text{Se}_3$  nanoplates. An ultrahigh refractive index has been observed in bulk  $\text{Bi}_{1.5}\text{Sb}_{0.5}\text{Te}_{1.8}\text{Se}_{1.2}$  crystals as well as in  $\text{Sb}_2\text{Te}_3$  thin films.[16, 17] These excellent optical properties mean that topological insulator materials are suitable for various optoelectronic devices, including plasmonic solar cells, ultrathin holograms, plasmonic and Fresnel lens, broadband photodetectors, and nanoscale waveguides. In this chapter, we focus on the excellent electronic and optical properties of topological insulator materials and their wide applications in advanced optoelectronic devices.[18]

## **1. Excellent electronic properties**

### **1.1 Quantum spin Hall effect**

The quantum spin Hall effect in two-dimensional (2D) topological insulators (TIs) was first proposed by Kane and Zhang.[19, 20] Later, this novel effect was predicted in mercury telluride–cadmium telluride (HgTe/CdTe) semiconductor quantum wells.[9] The HgTe/CdTe quantum wells have well-known strong spin-orbital coupling. When the thickness of the HgTe layer is smaller than 6.3 nm, the 2D electronic states have the normal band order, but when the thickness is larger than 6.3 nm, the 2D bands have an inversion, with a quantum phase transition between the ordinary insulator and the quantum spin Hall insulator.

The quantum spin Hall effect was experimentally realized in HgTe quantum wells in 2007.[21] In the quantum well, two edge states with opposite spin polarization counterpropagate at opposite edges. The quantum well also has non-local edge channel transport in the quantum spin Hall regime at zero external magnetic field.[22] Measurements of these properties confirmed that the quantum transport through the helical edge channels is non-dissipative. Nor can the topological protection of the edge states be destroyed by weak time-reversal symmetric perturbations. The electrons in edge states show an absence of elastic backscattering and robustness against disorder for surface transport.

Recently, bismuthene on a SiC substrate has been discovered as a candidate for a high-temperature quantum spin Hall material.[23] In general, quantum spin Hall materials require cryogenic temperatures due to their small energy gaps. Reis et al. showed that monolayer bismuth with honeycomb lattice on SiC(0001) has a band gap of  $\sim 0.8$  eV and conductive edge states. Their results demonstrated that this is a large-band-gap quantum spin Hall

material with its Fermi surface residing in the gap. This can ensure robust edge conductance at high temperature and can be used for designing and fabricating room-temperature non-dissipative quantum computing devices. The quantum spin Hall effect has also been observed at 100 K in a monolayer  $\text{WTe}_2$  crystal.[24] In the short-edge limit, monolayer  $\text{WTe}_2$  exhibits the hallmark transport conductance,  $\sim e^2/h$  per edge. The conductance can be suppressed by an external magnetic field, and a Zeeman-type gap can be opened. The results show the existence of a Kramers degenerate point and the importance of time-reversal symmetry for protection against elastic backscattering.

## 1.2 Topological magnetoelectric effects

The topological magnetoelectric effect is the phenomenon of magnetic polarization induced by applying an external electric field, or electric polarization induced by applying an external magnetic field. To obtain the topological magnetoelectric effect, a time-reversal-symmetry-breaking gap for the side surface is necessary.[25] A ferromagnetic layer with magnetization pointing out of the cylinder's surface induces a gap on the surface of the topological insulator, which has a fixed Hall conductance,  $\sigma_H = (n + 1/2) e^2/h$ , where  $e$  is the electronic charge and  $h$  is Planck's constant. When an electric field is applied parallel to the cylinder, a circulating current  $j$  can be induced on the interface. This current is identical to the current generated by a constant magnetization  $M$  that is anti-parallel to the electric field  $E$ . On the contrary, when a magnetic field  $B$  is applied parallel to the cylinder, a circulating current is produced parallel to the interface, which induces a Hall current  $j$  parallel or anti-parallel to the magnetic field  $B$ . As a result, charge density is accumulated on the top and bottom surfaces and induces the charge polarization.[2]

## 1.3 Magnetic monopole images

The topological magnetoelectric effect can be used to generate a magnetic monopole image through placing an electric charge near a topological surface state.[26] When an electric charge is put on the surface of a three-dimensional (3D) topological insulator with gapped surface states by time-reversal-symmetry breaking, the electric charge will polarize the bulk dielectric, and an image electric charge appears inside the topological insulator. An image magnetic monopole will also appear inside the topological insulator.[26]

The magnetic field generated by the image magnetic monopole has been experimentally measured and can be observed by a magnetic force microscope. A scanning magnetic force microscope tip can be applied to detect the magnetic field distribution of the image monopole. The magnetic field contribution from the magnetic monopole can also dominate and be distinguished from the contribution from surface impurities and roughness.

#### **1.4 Topological superconductors**

When topological insulators are connected with ordinary superconductors, topological superconductors appear due to the correlated interface states and the proximity effect.[27] Such topological superconductors are predicted to host Majorana fermion excitations.[1] A Majorana fermion is a fermion that is its own antiparticle and was first predicted in the 1930s. The zero-energy Majorana bound state is the simplest non-Abelian excitation and is associated with a vortex in a spinless superconductor. A Majorana zero mode has been proposed that can be realized in a superconducting vortex core by making use of the surface states of 3D topological insulators.[28] Topological protection and non-Abelian exchange statistics make the Majorana fermions promising for quantum computing. Signatures of Majorana fermions have been reported in quantum wires coupled to conventional superconductors.[29-31] Many experiments have been conducted to observe the elusive Majorana states.[30, 32]

Recently, a chiral Majorana fermion mode was observed in a quantum anomalous Hall insulator–superconductor structure.[33] This study demonstrated the existence of one-dimensional chiral Majorana fermion modes in the hybrid system of a quantum anomalous Hall insulator thin film coupled with a superconductor. The authors conducted transport measurements and found half-integer quantized conductance plateaus at the locations of magnetization reversals. The transport signature provided strong evidence of the Majorana fermion modes. The discovery of Majorana fermions could pave the way to topological quantum computing in the future.

#### **1.5 Quantum Anomalous Hall effects**

The topological surface states of 3D topological insulators are protected by time-reversal symmetry and are robust against non-magnetic disorder. Nevertheless, surface states open up a gap in the presence of time-reversal symmetry-breaking perturbations, and the Dirac

electrons become massive. Long range ferromagnetism interaction can break the time reversal symmetry.[34-37] Magnetic impurities such as Fe, Co, and Mn dopants will induce a surface state gap. Moreover, theoretically, the quantized anomalous Hall effect can emerge in magnetic topological insulators.[38]

Such a quantum anomalous Hall effect was observed experimentally soon after it was theoretically predicted in thin films of chromium-doped  $(\text{Bi,Sb})_2\text{Te}_3$ . [39] The gate-tuned anomalous Hall resistance reaches the predicted quantized value of  $h/e^2$  at zero magnetic field. Under a strong magnetic field, the longitudinal resistance vanishes, whereas the Hall resistance remains at the quantized value. The realization of the quantum anomalous Hall effect could lead to the development of next-generation low-power-consumption electronics.

In addition, Dirac spin-gapless semiconductors are another promising platform for the quantum anomalous spin Hall effect.[40, 41] Wang proposed that spin-gapless materials with linear energy dispersion are unique materials that can realize these massless and dissipationless states.[42] Monolayer ferromagnetic spin-gapless semiconductors such as MnO,  $\text{VO}_2$ , and CoO were proposed to realize the quantum anomalous Hall effect. In addition, 2D materials such as graphene, silicene, germanene, and stanene, as well as systems with transition metal oxides, have also been predicted as quantum anomalous Hall materials.[43]

## **1.6 Giant magnetoresistance effects**

Electronic transport is significant not only for obtaining a fundamental understanding of the electronic properties of materials, but also for promoting their applications in practical electronic and optoelectronic devices.[44-47] Giant magnetoresistance and quantum oscillations have been reported in a variety of 3D topological insulators.[48-54] The Dirac fermions of surface states suggest enhanced quantum corrections of magnetoconductance.[55] Spin-momentum locked surface states always show a weak antilocalization effect due to strong spin-orbit coupling. Aharonov–Bohm oscillations have also been observed in  $\text{Bi}_2\text{Se}_3$  and  $\text{Bi}_{1-x}\text{Sb}_x$  topological insulators.[56, 57] Non-saturating positive linear magnetoresistance (MR) at high fields was observed in  $\text{Bi}_2\text{Te}_3$  films and  $\text{Bi}_2\text{Se}_3$  nanoribbons.[58-60] Room temperature giant and linear MR were observed in the topological insulator  $\text{Bi}_2\text{Te}_3$  in the form of nanosheets with a few quintuple layers.[61] The giant, linear magnetoresistance that was achieved was as high as over 600% at room

temperature, without any sign of saturation at measured fields up to 13 T. The observed linear magnetoresistance was attributed to the quantum linear magnetoresistance model developed by Abrikosov.[62, 63]

Actually, the transport behavior of topological insulators reflects the combined contributions of surface states and bulk states due to the metallic bulk. A weak localization effect emerges when the time reversal symmetry is broken and a gap opens in surface states.[64-66] Competition between a weak antilocalization effect and a weak localization effect has been observed in topological insulator thin film  $\text{Bi}_{1-x}\text{Cr}_x\text{Se}_3$  and  $(\text{Bi}_{0.57}\text{Sb}_{0.43})_2\text{Te}_3$ . [67-69] The weak localization effect has been attributed to the 2D quantized channels of bulk states.[69]

### **1.7 Shubnikov-de Haas effects**

The surface states of 3D topological insulators have high carrier mobility, and the Shubnikov-de Haas effect can appear in the presence of very intense magnetic fields.[70] The Shubnikov-de Haas effect is a macroscopic manifestation of the inherent quantum mechanical nature of matter. The Shubnikov-de Haas effect is a convincing tool for characterizing quantum transport in electronic materials.[71] It can be used to isolate the surface carriers and to determine their mobility and effective mass.[72] Shubnikov-de Haas effects were first observed in 3D topological insulator  $\text{Bi}_2\text{Te}_3$  single crystals, as shown in Fig. 1.28 in Ref. [56]. Surface mobility of up to 9000 to 10,000  $\text{cm}^2/\text{V}\cdot\text{s}$  was obtained based on Shubnikov-de Haas quantum oscillations, which is substantially higher than in the bulk. The obtained Fermi velocity of  $4 \times 10^5$  m/s agrees with the results from angle-resolved photoemission measurements. Shubnikov-de Haas quantum oscillations have also been observed in 3D topological insulators,  $\text{Bi}_2\text{Te}_2\text{Se}$  crystals,  $\text{Bi}_2\text{Te}_3$  nanowires, and YPdBi crystals.[70, 73, 74]

## **2. Excellent optical properties**

### **2.1 Ultrahigh bulk refractive index**

Apart from their fascinating electronic properties, a variety of excellent optical properties have been discovered in topological insulator materials. Optical constants are the basic optical parameters of materials, which define the interactions of incident light and materials. The refractive index  $n$  and the extinction coefficient  $k$  of cleaved flat  $\text{Bi}_{1.5}\text{Sb}_{0.5}\text{Te}_{1.8}\text{Se}_{1.2}$  crystal sheets were measured by using a spectroscopic ellipsometer. The  $\text{Bi}_{1.5}\text{Sb}_{0.5}\text{Te}_{1.8}\text{Se}_{1.2}$

crystal features low refractive index in the surface but ultrahigh refractive index in the bulk in the near infrared frequency range (Figure 1).[16] This excellent optical property makes topological insulator materials promising for designing novel near-infrared optoelectronic devices.[75-77]

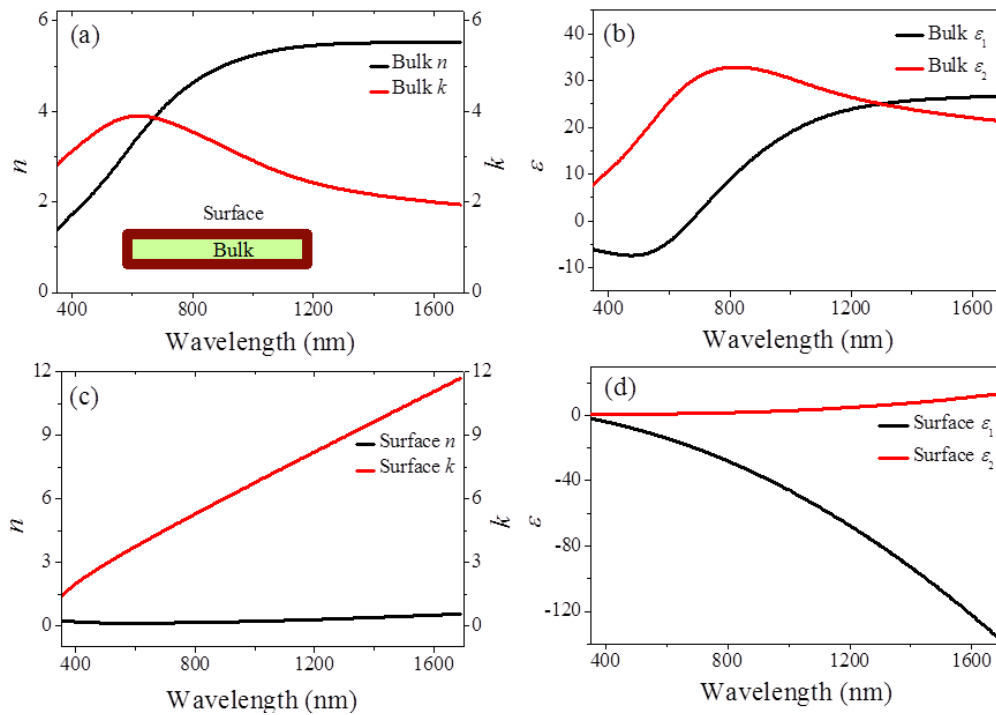


Figure 1. Optical parameters of  $\text{Bi}_{1.5}\text{Sb}_{0.5}\text{Te}_{1.8}\text{Se}_{1.2}$  single crystals. (a-b) Refractive index  $n$ , extinction coefficient  $k$ , and dielectric function  $\epsilon$  of the insulating bulk of  $\text{Bi}_{1.5}\text{Sb}_{0.5}\text{Te}_{1.8}\text{Se}_{1.2}$  crystals. (c-d) Refractive index  $n$ , extinction coefficient  $k$ , and dielectric function  $\epsilon$  of the metallic surface of  $\text{Bi}_{1.5}\text{Sb}_{0.5}\text{Te}_{1.8}\text{Se}_{1.2}$  crystals. Reprinted with permission from [Yue, 2016], Science Advances 2 (2016) e1501536. © 2017, AAAS.

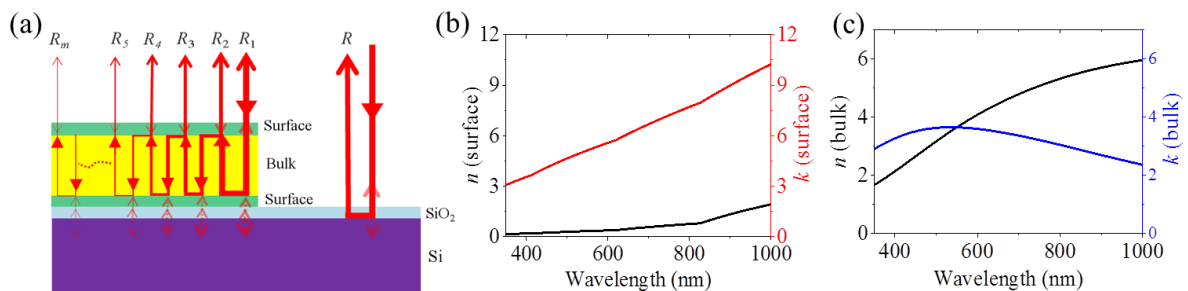


Figure 2. Physical mechanism of the  $\text{Sb}_2\text{Te}_3$  thin film cavity. (a) Diagram of internal light multiple reflections in the resonant cavity of the  $\text{Sb}_2\text{Te}_3$  thin film. The refractive index  $n$  (b) and extinction coefficient  $k$  (c) of the surface and bulk of  $\text{Sb}_2\text{Te}_3$  thin film. Reprinted with permission from [Yue, 2017], Nature Communications, 8 (2017) 15354. © 2017 Macmillan Publishers Limited, part of Springer Nature.

In additions, the unequal refractive index in the surface and bulk of topological insulator thin films could generate an intrinsic resonant cavity.[17] The multilayer structure of the  $\text{Sb}_2\text{Te}_3$  thin film on a Si substrate is schematically shown in Figure 2(a). The dielectric bulk of the  $\text{Sb}_2\text{Te}_3$  thin film is sandwiched within the two metallic surface layers. The refractive index  $n$  and extinction coefficient  $k$  of the surface layers and the bulk are unequal due to their different electronic properties. With the unequal refractive index, the  $\text{Sb}_2\text{Te}_3$  thin film acts as an intrinsic optical resonant cavity.[78] Two surface layers serve as two reflectors. The bulk behaves as an optical resonant cavity. Thus, an incident light beam can be reflected multiple times between the two surface layers and be partially confined in the bulk. The phase modulation of the reflected light beam from the resonant cavity can be enhanced. This unique function could be of benefit for many optoelectronic devices that rely on phase shifts such as holography and Fresnel lenses.

## 2.2 Near-infrared transparency

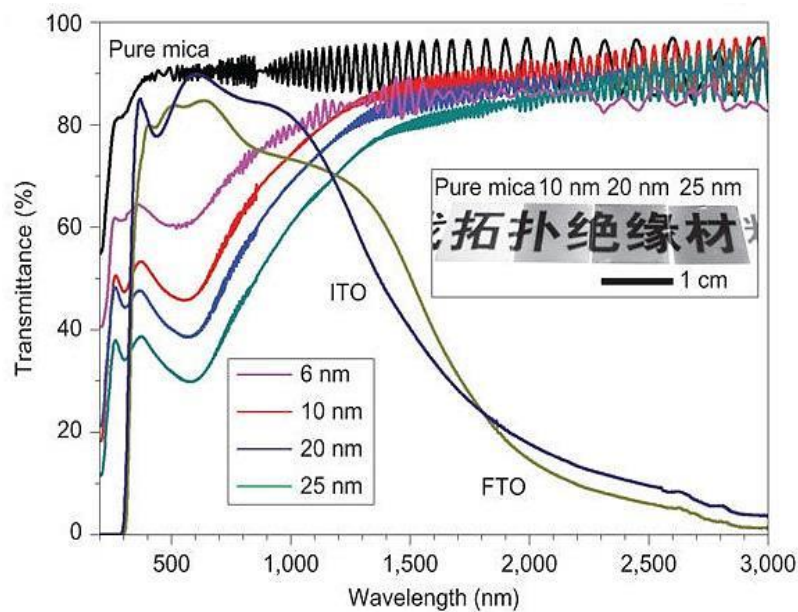


Figure 3. Spectroscopy characterization of  $\text{Bi}_2\text{Se}_3$  nanosheets on thin mica sheet substrates. Ultraviolet–visible–infrared spectra of  $\text{Bi}_2\text{Se}_3$  nanosheets with different thicknesses, mica



substrate, indium tin oxide (ITO), and fluorine tin oxide (FTO). The obvious oscillatory behavior in the transmission spectra may be a result of Fabry–Perot interference effects. Reprinted with permission from [Peng, 2012], Nature Chemistry 4 (2012) 281–286. © 2012 Macmillan Publishers Limited, part of Springer Nature.

Near-infrared transparent flexible electrodes based on few-layer  $\text{Bi}_2\text{Se}_3$  nanostructures on mica were demonstrated. It was found that the  $\text{Bi}_2\text{Se}_3$  nanosheets exhibit a transparency of more than 70% over a wide range of wavelengths. Furthermore, the  $\text{Bi}_2\text{Se}_3$  nanosheets were used as transparent electrodes. The electrodes showed high chemical and thermal stability as well as excellent mechanical durability. These features make the  $\text{Bi}_2\text{Se}_3$  nanosheets promising candidates for novel optoelectronic devices.[79] In addition, with their ultrahigh refractive index, the topological insulator nanosheets are also useful for designing transparent optical devices such as ultrathin flat lenses and light modulators.

### **2.3 Faraday rotation and unusual electromagnetic scattering**

Faraday rotation was predicted in topological insulator surfaces.[25] It results from topological magnetoelectric effects in magnetic topological insulators. In principle, it is possible to find a topological insulator with a larger gap which could support an accurate measurement of Faraday rotation. Similar proposals can also be worked out for the rotation of the reflected wave Kerr effect. In addition, it is possible to replace the ferromagnetic layers by paramagnetic materials with large susceptibilities and apply an external magnetic field to polarize them. In this case the magnetization is proportional to the magnetic field, such that the Faraday rotation contributed by the bulk is also proportional to the magnetic field. Unusual electromagnetic scattering was predicted from topological insulator nanoparticles.[80]

### **2.4 Ultra-broadband plasmon excitations**

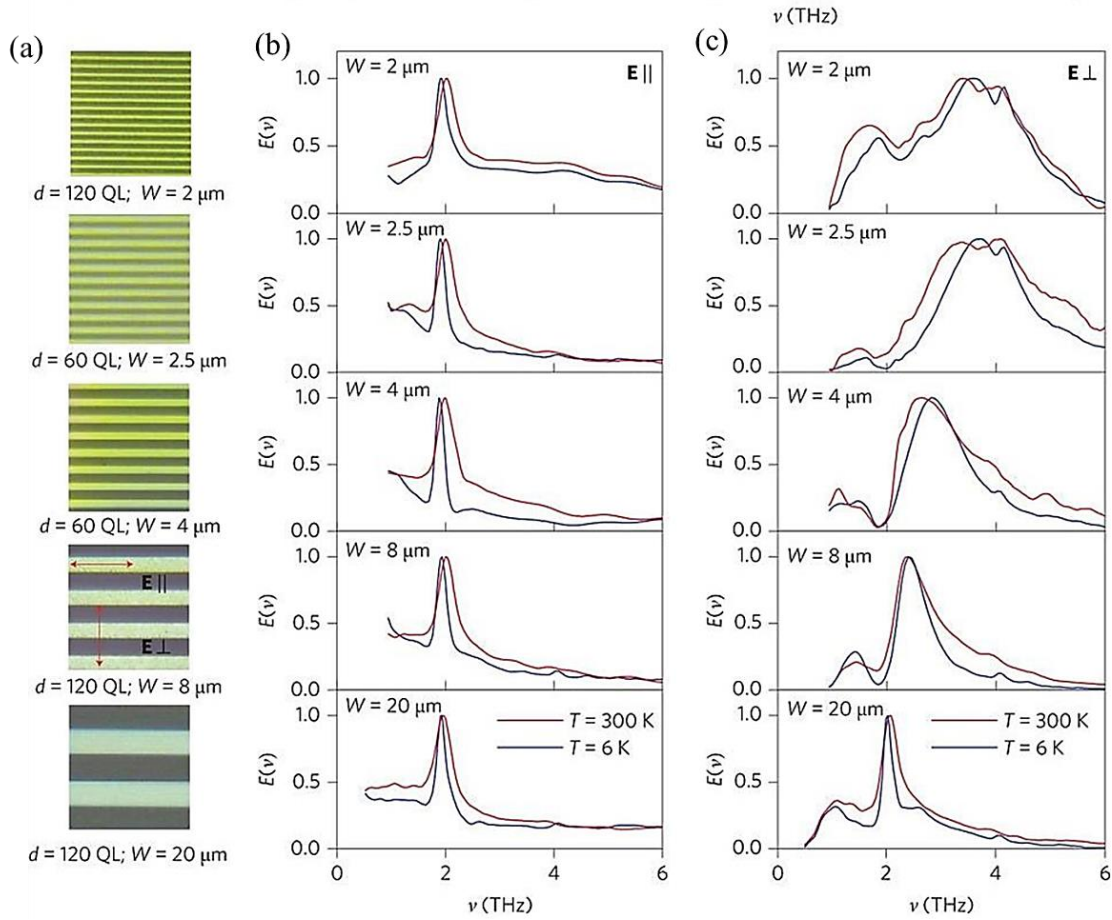


Figure 4. Extinction coefficients of the micro-ribbon arrays of topological insulator  $\text{Bi}_2\text{Se}_3$  in the terahertz range. (a) Optical microscope image of 5 patterned films with different widths and periods. Extinction coefficients of the 5 patterned films with the radiation electric field applied in directions (b) parallel and (c) perpendicular to the ribbons. Reprinted with permission from [Yue, 2013], Nature Nanotechnology 8 (2013) 556–560. © 2013 Macmillan Publishers Limited, part of Springer Nature.

Plasmons are quantized collective oscillations of electrons and have been mainly observed and investigated in noble metals. Plasmons have been widely applied in various optical devices from ultraviolet to THz frequencies.[81-83] Dirac plasmons from massless electrons are promising for novel tunable plasmonic devices. They exist in 2D materials such as graphene and semiconductors. Dirac plasmon excitations have also been observed in binary  $\text{Bi}_2\text{Se}_3$  at THz frequencies.[14] The  $\text{Bi}_2\text{Se}_3$  was prepared in thin micro-ribbon arrays of different widths and periods. The linewidth of the plasmon was found to remain nearly constant at temperatures between 6 K and 300 K. Sim *et al.* also reported a large modulation depth of 2,400% at 1.5 THz in micro-ribbon arrays of topological insulator  $\text{Bi}_2\text{Se}_3$  with very low optical fluence of  $45 \text{ }\mu\text{J cm}^{-2}$ .[84]

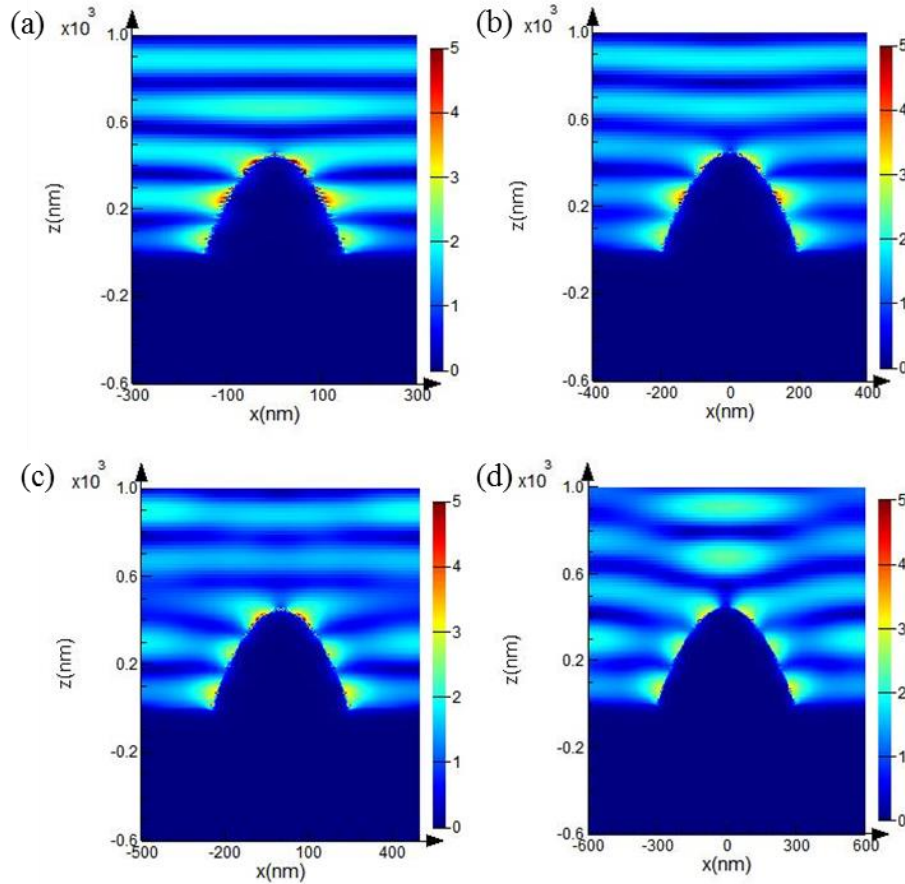


Figure 5. Simulation of the electromagnetic field distribution in  $\text{Bi}_{1.5}\text{Sb}_{0.5}\text{Te}_{1.8}\text{Se}_{1.2}$  nanocone arrays using the finite-difference time-domain (FDTD) method. The plasmon resonances are localized and enhanced on the surfaces of  $\text{Bi}_{1.5}\text{Sb}_{0.5}\text{Te}_{1.8}\text{Se}_{1.2}$  nanocones. The nanocone arrays have variable diameters and periods. Reprinted with permission from [Yue, 2016], Science Advances 2 (2016) e1501536. © 2017, AAAS.

Ultraviolet and visible frequency plasmonics have been observed in nanoslit arrays and gratings of bulk-insulating  $\text{Bi}_{1.5}\text{Sb}_{0.5}\text{Te}_{1.8}\text{Se}_{1.2}$  crystals.[15, 16] A conic nanostructure made of  $\text{Bi}_{1.5}\text{Sb}_{0.5}\text{Te}_{1.8}\text{Se}_{1.2}$  crystals was fabricated using focused ion beam lithography. The insulating bulk showed an ultrahigh refractive index of up to 5.5 in the near-infrared frequency range. The metallic surface presented plasmonic excitations and strong backward light scattering in the visible frequency range. Through integrating the nanocone arrays into a-Si thin film solar cells, up to 15% enhancement of light absorption was obtained.

Actively tunable visible surface plasmons in  $\text{Bi}_2\text{Te}_3$  nanoplates were studied by electron energy-loss spectroscopy and cathodoluminescence spectroscopy.[85, 86] The observed plasmons in the visible range were mainly from metallic surface states of  $\text{Bi}_2\text{Te}_3$ . Infrared

nanoimaging of surface metallic plasmons in  $\text{Bi}_2\text{Te}_3$  nanoplates was also studied using scattering-type scanning near-field optical microscopy.[87] Near-field patterns of bright outside fringes were also discovered, which originated from the surface-metallic plasmonic behavior at mid-infrared frequency.

With their metallic surfaces and insulating bulk, topological insulator materials provide an excellent platform for the realization of a new type of nanostructure that could combine the fascinating properties of plasmonic metallic nanostructures and dielectric nanostructures. With these features, the plasmonic topological insulator nanostructures could pave the way to the design of low-loss and high-performance optical devices, such as visible to infrared detectors or sensors.[88, 89]

## **2.5 Polarized light induced photocurrent**

The control of topological insulator photocurrents by light has been investigated.[90] It was shown that illuminating the  $\text{Bi}_2\text{Se}_3$  with circularly polarized light generates a photocurrent that originates from topological helical Dirac fermions, and that reversing the helicity of the light reverses the direction of the photocurrent. The authors also observed a photocurrent that could be controlled by the linear polarization of light and argued that it may also have a topological surface state origin. This approach may allow the probing of dynamic properties of topological insulators and lead to novel opto-spintronic devices.

## **2.6 Broadband optical nonlinear response**

The nonlinear response of  $\text{Bi}_2\text{Te}_3$  was studied at both optical and microwave wavelengths. The researchers demonstrated the optical saturable absorption property of  $\text{Bi}_2\text{Te}_3$  from 800 nm to 1550 nm.  $\text{Bi}_2\text{Te}_3$  shows a saturation intensity of  $\sim 12 \mu\text{W}/\text{cm}^2$  and a normalized modulation depth of  $\sim 70\%$ . They argued that the optical saturable absorption in TI is a natural consequence of the Pauli-blocking principle of the electron filling in the bulk insulating state.[91]

Electromagnetically-induced transparency was found in  $\text{Bi}_2\text{Se}_3$  under the application of a strong THz electric field. This effect, concomitantly determined by harmonic generation and charge-mobility reduction, is exclusively related to the presence of Dirac electrons at the surface of  $\text{Bi}_2\text{Se}_3$ , and opens the way towards tunable THz nonlinear optical devices based on TI materials.[92] The third order nonlinear optical property of  $\text{Bi}_2\text{Se}_3$  was also investigated under femtosecond laser excitation.[93] When excited at 800 nm, the TI  $\text{Bi}_2\text{Se}_3$

exhibits saturable absorption with a saturation intensity of  $10.12 \text{ GW/cm}^2$ , a modulation depth of 61.2%, and a giant nonlinear refractive index of  $10^{-14} \text{ m}^2/\text{W}$ . This work suggested that  $\text{Bi}_2\text{Se}_3$  is a promising nonlinear optical material and can find potential applications ranging from passive laser mode lockers to optical Kerr effect based photonic devices.

### 3. Advanced optoelectronic devices

#### 3.1 Plasmonic solar cells

Topological insulator nanocone arrays can combine the excellent properties of plasmonic metallic nanostructures and high-refractive-index dielectric nanostructures.[16] They feature both localized surface plasmonic resonances and strong light scattering. Because the plasmonic resonances in the nanocone arrays are located in the visible frequency range, integrating them into photovoltaic devices is expected to achieve enhanced light absorption and efficiency. The strong backward scattering in the nanocone arrays also enables the enhancement of optical absorption when they are placed at the back of photovoltaic devices.

Using the finite-difference time-domain (FDTD) method, they theoretically simulated the enhancement of light absorption in a 300-nm-thick a-Si solar cell. The configuration of the proposed a-Si thin film solar cells is shown in Figure 6a. With the integration of topological insulator nanoparticles, a large light absorption enhancement was achieved in both the short wavelength and long wavelength regions (Figure 6b). These results indicate the potential application of the topological insulator nanocone arrays in solar cell technology.

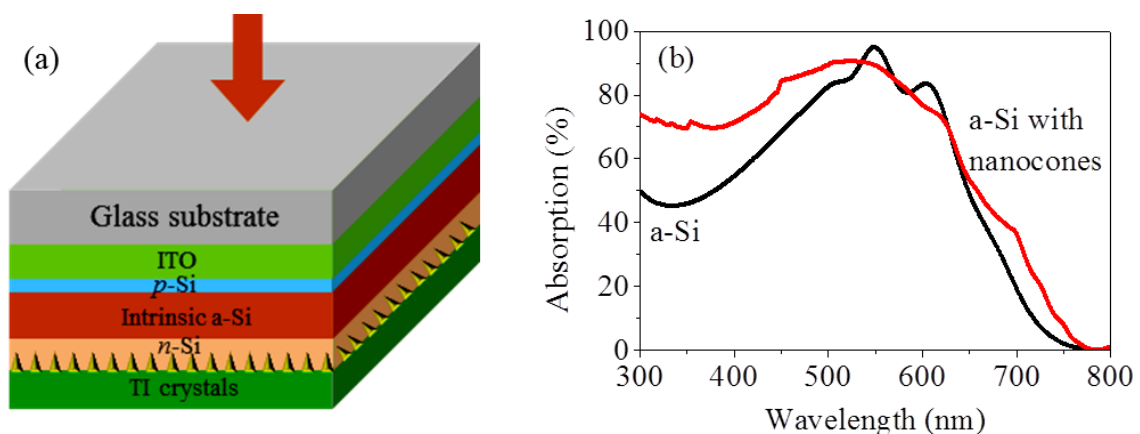


Figure 6. Plasmon resonance enhanced light absorption in ultrathin a-Si solar cells simulated using FDTD. (a) Structure of ultrathin a-Si solar cells with  $\text{Bi}_{1.5}\text{Sb}_{0.5}\text{Te}_{1.8}\text{Se}_{1.2}$  nanocone arrays. (b) The arrays achieve broadband enhancement of light absorption in the visible

frequency range. Reprinted with permission from [Yue, 2016], *Science Advances* 2 (2016) e1501536. © 2017, AAAS.

### 3.2 Nanometric holograms

It was found that nanometric topological insulator thin films act as intrinsic optical resonant cavities due to the unequal refractive indices in their metallic surfaces and bulk.[17] The resonant cavity leads to enhancement of phase shifts and thus holographic imaging. The researchers designed and fabricated an ultrathin hologram using the direct laser writing method on topological insulator  $\text{Sb}_2\text{Te}_3$  thin film. The laser selectively removed thin films based on the calculated hologram patterns and created a binary hologram. The hologram was as thin as 25 nm and could achieve high quality full colour images in a layer 60 nm thick (Figure 7). The 25 nm hologram is the world's thinnest hologram. This work paves the way towards integrating holography with flat electronic devices for optical imaging, data storage, and information security. Especially, they are promising for realizing 3D holographic smartphones and smartwatches.

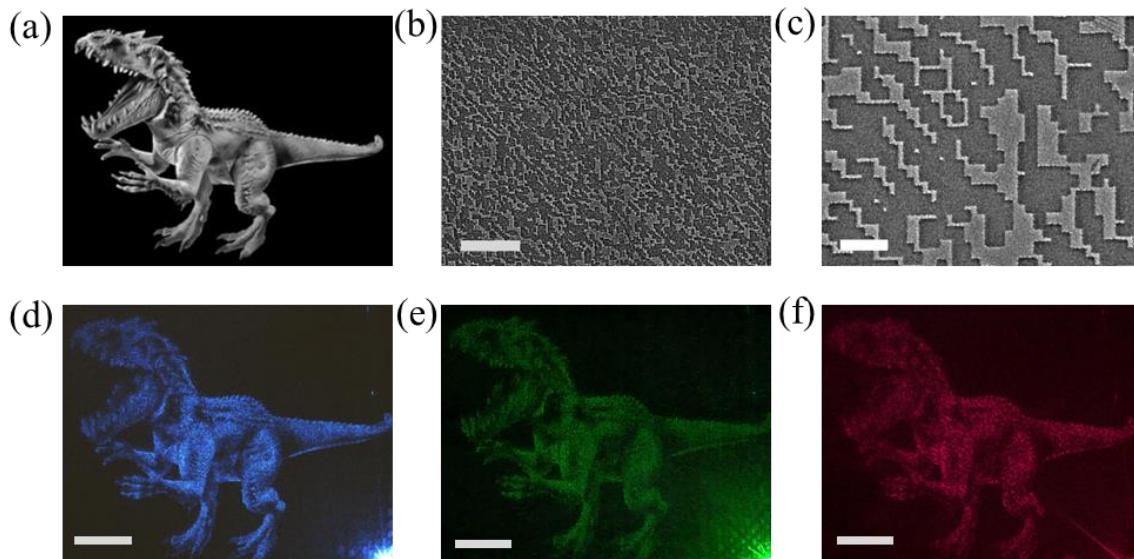


Figure 7. Nanometric  $\text{Sb}_2\text{Te}_3$  thin film holograms and reconstructed images. (a) Original image of the dinosaur object. (b-c) SEM images of the laser printed hologram patterns. (d-f) Holographic images captured by illuminating the nanometric holograms using 445, 532, and 632 nm continuous wave laser beams. Reprinted with permission from [Yue, 2017], *Nature Communications*, 8 (2017) 15354. © 2017 Macmillan Publishers Limited, part of Springer Nature.

### 3.3 Ultrathin flat lens

An ultrathin double-focusing lens, capable of simultaneously generating a plasmonic focus in the near-field region and a Fresnel-zone-plate based diffraction-limited focal spot in the far-field region, was designed using  $\text{Sb}_2\text{Te}_3$  thin films.[94] The  $\text{Sb}_2\text{Te}_3$  thin films have a high refractive index in the bulk and plasmonic excitations on the surface.[95] The plasmonic lens is able to redirect the surface plasmon polaritons and create a plasmonic focus in the near-field regime. Since the plasmonic field coupled with the light has a smaller wavelength, the generated plasmonic focus has a smaller size that is beyond the diffraction limit. On the other hand, the Fresnel lens, consisting of radially-symmetric binary zones, is capable of focusing the diffracted light beams into a diffraction-limited focal spot in the far-field regime. The double-focusing flat lens opens up new opportunities for future compact devices with versatile functionalities, with potential applications ranging from optical imaging to information technology.

### 3.4 Near-infrared photodetector

Photodetectors are sensors of light, which can convert light photons into photocurrent or photovoltage.[96-99] Topological insulators have an energy gap in the bulk and a gapless surface state consisting of a single Dirac cone. Low-frequency optical absorption due to the surface state is universally determined by the fine-structure constant. When the thickness of these 3D topological insulators is reduced, they become quasi-two-dimensional insulators with enhanced absorbance. The two-dimensional insulators can be topologically trivial or nontrivial depending on their thickness, and we predict that the optical absorption is larger for the topological nontrivial case compared with the trivial case. Since the surface state is intrinsically gapless, we propose its potential application in wide bandwidth, high-performance photodetection, covering a broad spectrum ranging from terahertz to infrared. The photodetection performance can be dramatically enhanced when the thickness is reduced to several quintuple layers with a widely tunable band gap depending on the thickness.[18]

A high performance broadband photodetector was reported based on  $\text{Bi}_2\text{Se}_3$  nanowires.[100]  $\text{Bi}_2\text{Se}_3$  nanowires were fabricated using the focused ion beam technique and can be used for ultrasensitive visible–near-infrared (IR) photodetectors. The authors observed efficient electron-hole pair generation in the  $\text{Bi}_2\text{Se}_3$  nanowire under illumination by visible (532 nm) and IR light (1064 nm). They observed photoresponsivity of up to 300 A/W. The terahertz/infrared radiation induced photogalvanic effect was found to exist in

$(\text{Bi}_{1-x}\text{Sb}_x)_2\text{Te}_3$ . [101] They found that the observed photogalvanic effect is sensitive to the surface symmetry and scattering details, and can be applied to study the high frequency conductivity of the surface states. In particular, measuring the polarization dependence of the photogalvanic current and scanning with a micrometer-sized beam spot across the sample provide access to topographical inhomogeneities in the electronic properties of the surface states and the local domain orientation.

A near-infrared light photodetector was fabricated based on a  $\text{Sb}_2\text{Te}_3$  thin film, which was grown on sapphire by molecular beam epitaxy (MBE). Electrical analysis revealed that the resistance of the film decreases with increasing temperature in the temperature range of 8.5–300 K. Further optoelectronic characterization showed that the as-fabricated photodetector exhibits obvious sensitivity to 980 nm light illumination. The responsivity, photoconductive gain, and detectivity were estimated to be 21.7 A/W, 27.4, and  $1.22 \times 10^{11}$  Jones, respectively, which are much better than those of other topological insulator based devices. This study suggests that the present near-IR (NIR) photodetector may have potential applications in future optoelectronic devices. [102]

### **3.5 Saturable absorber**

Topological insulator  $\text{Bi}_2\text{Te}_3$  can serve as a saturable absorber with high modulation depth at 1.55  $\mu\text{m}$  (Figure 8). A  $\text{Bi}_2\text{Te}_3$  based saturable absorber device was fabricated and used as a passive mode locker for ultrafast pulse formation in the telecommunications band. [103] 3- $\mu\text{m}$  mid-infrared pulses were also generated using the  $\text{Bi}_2\text{Te}_3$  as the saturable absorber. [104] The  $\text{Bi}_2\text{Te}_3$  shows a low saturable peak intensity of 2.12  $\text{MW}/\text{cm}^2$  and a high modulation depth of 51.3%. The bulk-structured  $\text{Bi}_2\text{Te}_3$  layer can provide sufficient nonlinear saturable absorption for femtosecond mode-locking. [105] The researchers used the  $\text{Bi}_2\text{Te}_3$  as an ultrafast mode-locker to generate femtosecond pulses from an all-fiberized cavity. They demonstrated that stable soliton pulses with a temporal width of ~600 femtosecond could be produced at 1.55  $\mu\text{m}$  from an erbium fiber ring cavity.



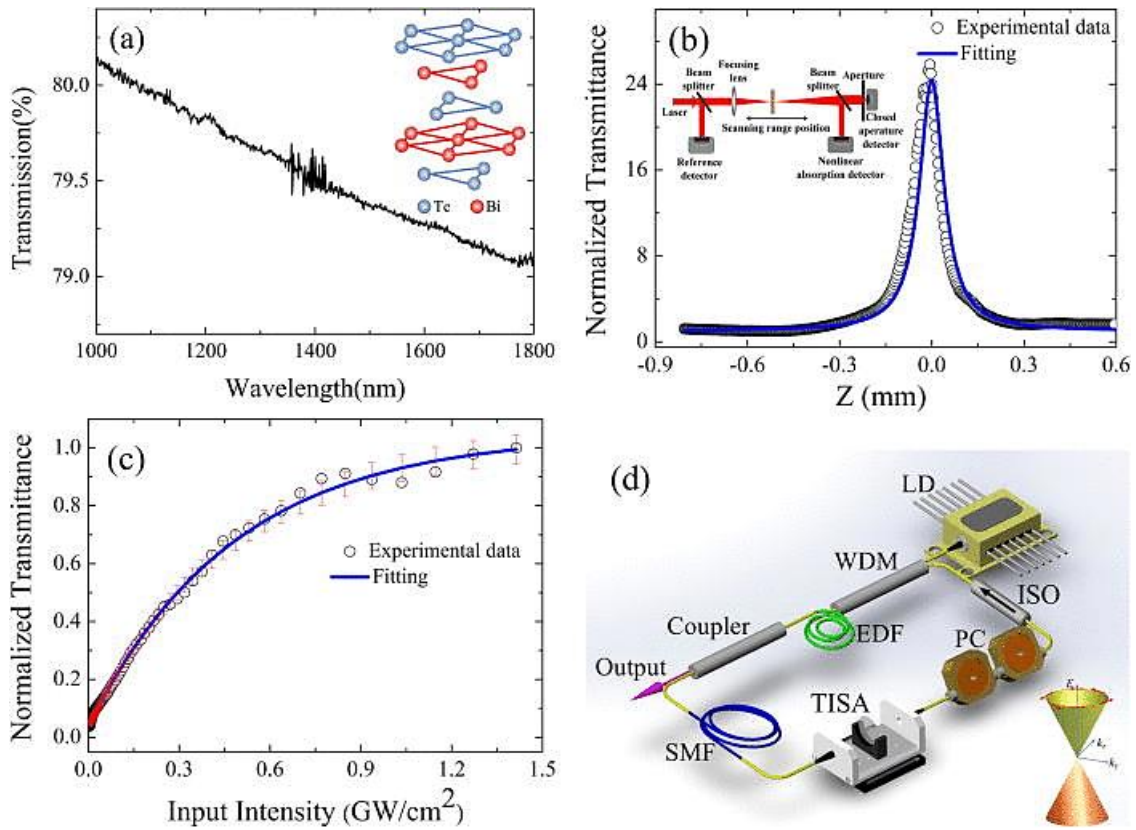


Figure 8. Ultra-short pulse generation by topological insulator material  $\text{Bi}_2\text{Te}_3$  that works as a saturable absorber. (a) The near infrared linear absorption spectrum of the  $\text{Bi}_2\text{Te}_3$ . (b) A typical Z-scan peak curve of  $\text{Bi}_2\text{Te}_3$  at 1550 nm; inset: measurement configuration. (c) The corresponding nonlinear saturable absorption curve. (d) Schematic illustration of the fiber laser. Reprinted with permission from [Yue, 2012], *Apply Physics Letter* 101 (2012) 211106. © 2012 AIP Publishing LLC.

A high-energy, wavelength-tunable, Q-switched erbium-doped fiber laser was fabricated using the  $\text{Bi}_2\text{Te}_3$ . [106] The saturation intensity was  $\sim 57 \text{ MW/cm}^2$ , and the modulation depth was  $\sim 22\%$ . The single pulse energy is  $\sim 1.5 \mu\text{J}$ , and the saturable absorption operation from  $\sim 1.51 \mu\text{m}$  to  $\sim 1.58 \mu\text{m}$ . A 2 GHz passively harmonic mode-locked fiber laser was also constructed with a microfiber-based  $\text{Bi}_2\text{Te}_3$  saturable absorber. [107] The fiber laser could operate at the pulse repetition rate of 2.04 GHz under a pump power of 126 mW.  $\text{Bi}_2\text{Te}_3$  nanoparticles have exhibited broadband saturable absorption at  $0.8 \mu\text{m}$  and  $1.57 \mu\text{m}$ . They were employed as nonlinear saturable absorbers to passively mode-lock the erbium-doped fiber lasers for sub-400 fs pulse generation. [108] The  $\text{Bi}_2\text{Te}_3$  exhibited a nonlinear absorption response. [109] The  $\text{Bi}_2\text{Te}_3$  sheets showed saturation absorption intensity of

1.1 W/cm<sup>2</sup> at 1.0 μm. A Q-switching pulsed laser was constructed from a 1.0 μm Nd:YVO<sub>4</sub> laser, where the threshold absorbed pump power was 31 mW. A pulse duration of 97 ns was observed with an average power of 26.1 mW. A Q-switched laser at 1.3 μm was also realized with a pulse duration of 93 ns.

The topological insulator Bi<sub>2</sub>Se<sub>3</sub> demonstrated the capability to modulate the operation of a bulk solid-state laser by taking advantage of its saturable absorption. They are potentially attractive as broadband pulsed modulators for the generation of short and ultrashort pulses in bulk solid-state lasers.[110] A wavelength-tunable picosecond soliton fiber laser was achieved using the topological insulator material Bi<sub>2</sub>Se<sub>3</sub> as a mode locker.[111] An optical pulse of ~660 fs was generated at a wavelength of 1.55 μm. A modulation depth of 98% and a saturation intensity of 0.49 GW/cm<sup>2</sup> were observed. Femtosecond pulses were also generated from Bi<sub>2</sub>Se<sub>3</sub> mode-locked fiber laser.[112] The Bi<sub>2</sub>Se<sub>3</sub> saturable absorber that was used has a low saturable optical intensity of 12 MW/cm<sup>2</sup> and a modulation depth of ~3.9%. The mode-locking operation was realized at 25 mW. A mode-locked ytterbium-doped fiber laser was fabricated based on the Bi<sub>2</sub>Se<sub>3</sub>. [113] The measured modulation depth of the Bi<sub>2</sub>Se<sub>3</sub> film was 5.2%. When the Bi<sub>2</sub>Se<sub>3</sub> film was used in the Yb-doped fiber laser, the mode locked pulses had pulse energy of 0.756 nJ, pulse width of 46 ps, and the repetition rate of 44.6 MHz. The maximum average output power was 33.7 mW. When the pump power exceeded 270 mW, the laser could operate in a multiple pulse state, so that a six-pulse regime could be realized.

A high-repetition-rate Q-switched fiber laser was made using the Bi<sub>2</sub>Se<sub>3</sub> film.[114] The Bi<sub>2</sub>Se<sub>3</sub> film had a low saturable optical intensity of 11 MW/cm<sup>2</sup>. By inserting the absorber film into an Erbium-doped fiber laser, a high-repetition Q-switched laser with repetition rates from 459 kHz to 940 kHz was achieved. The maximum output power was 22.35 mW with shortest pulse duration of 1.9 μs. A 1.06 μm Q-switched ytterbium-doped fiber laser was made using few-layer Bi<sub>2</sub>Se<sub>3</sub> as a saturable absorber.[114] The few-layer Bi<sub>2</sub>Se<sub>3</sub> had a low saturable optical intensity of 53 MW/cm<sup>2</sup>. By inserting Bi<sub>2</sub>Se<sub>3</sub> into an yttrium-doped fiber (YDF) laser cavity, stable Q-switching operation at 1.06 μm was achieved. The Q-switched pulses have pulse duration of 1.95 μs, a pulse energy of 17.9 nJ, and a tunable pulse-repetition-rate from 8.3 to 29.1 kHz. A Q-switched mode-locked erbium-doped fiber laser was designed based on the Bi<sub>2</sub>Se<sub>3</sub> deposited fiber taper.[115] Due to the low saturation intensity, stable Q-switched mode-locked fiber laser pulses centred at 1.56 μm can be generated at a pump power of 10 mW.

These results demonstrate that the topological insulator materials  $\text{Bi}_2\text{Te}_3$  and  $\text{Bi}_2\text{Se}_3$  are promising optical materials for constructing broadband, miniature, and integrated high-energy pulsed laser systems with low power consumption.

#### **4. Conclusion and outlook**

Topological insulator materials are a series of novel materials that feature topological metallic (edge) surface states and insulating bulk states. With a variety of excellent electronic and optical properties, they could find wide applications in future advanced optoelectronic devices. At present, however, there are still several challenges for developing high performance topological insulator based devices. The first is the quality of currently synthesised topological materials. The existing topological insulator materials mostly suffer from the problem of defect induced bulk conductivity that can mask the surface contribution. Some of the optical devices mentioned above are based on the electronic properties of both the bulk and the surface. This problem is expected to be solved through exploring large bulk gap topological materials and improving the synthesis technology. The second is the temperature problem. Some of the unique electronic properties such as the quantum spin Hall effect and quantum anomalous Hall effect that hold potential for non-dissipative quantum devices were only observed at very low temperature. In order to enable them suitable for practical applications, the temperature must be improved up to room temperature. In addition, the performance of recently developed topological insulator based optoelectronic devices, such as the ultrathin hologram and saturable absorber, still has much room for improvement. Overall, topological insulators are novel and unique materials with great potential for future electronic and optoelectronic devices. Through overcoming their existing problems, practical commercialized topological insulator based devices are foreseeable and can be realized in the near future.

#### **References**

- [1] M.Z. Hasan, C.L. Kane, Colloquium: Topological insulators, *Reviews of Modern Physics*, 82 (2010) 3045-3067.
- [2] X.-L. Qi, S.-C. Zhang, Topological insulators and superconductors, *Reviews of Modern Physics*, 83 (2011) 1057-1110.

- [3] Z. Yue, Electronic transport, magnetic and thermal properties of gapless materials, UoW PhD Thesis, 4138 (2013).
- [4] Y. Ando, Topological Insulator Materials, Journal of the Physical Society of Japan, 82 102001.
- [5] Z. Yue, Q. Chen, X. Wang, Thermoelectric signals of state transition in polycrystalline SmB<sub>6</sub>, Journal of Physics: Condensed Matter, 28 (2016) 355801.
- [6] Y.L. Chen, J.G. Analytis, J.-H. Chu, Z.K. Liu, S.-K. Mo, X.L. Qi, H.J. Zhang, D.H. Lu, X. Dai, Z. Fang, S.C. Zhang, I.R. Fisher, Z. Hussain, Z.-X. Shen, Experimental Realization of a Three-Dimensional Topological Insulator, Bi<sub>2</sub>Te<sub>3</sub>, Science, 325 (2009) 178-181.
- [7] H. Zhang, C.-X. Liu, X.-L. Qi, X. Dai, Z. Fang, S.-C. Zhang, Topological insulators in Bi<sub>2</sub>Se<sub>3</sub>, Bi<sub>2</sub>Te<sub>3</sub> and Sb<sub>2</sub>Te<sub>3</sub> with a single Dirac cone on the surface, Nat Phys, 5 (2009) 438-442.
- [8] Y. Ando, Topological Insulator Materials, Journal of the Physical Society of Japan, 82 (2013) 102001.
- [9] B.A. Bernevig, T.L. Hughes, S.-C. Zhang, Quantum Spin Hall Effect and Topological Phase Transition in HgTe Quantum Wells, Science, 314 (2006) 1757-1761.
- [10] D. Hsieh, D. Qian, L. Wray, Y. Xia, Y.S. Hor, R.J. Cava, M.Z. Hasan, A topological Dirac insulator in a quantum spin Hall phase, Nature, 452 (2008) 970-974.
- [11] J.E. Moore, The birth of topological insulators, Nature, 464 (2010) 194-198.
- [12] X.-L. Wang, S.X. Dou, C. Zhang, Zero-gap materials for future spintronics, electronics and optics, NPG Asia Mater, 2 (2010) 31-38.
- [13] A. Politano, L. Viti, M.S. Vitiello, Optoelectronic devices, plasmonics, and photonics with topological insulators, APL Materials, 5 (2017) 035504.
- [14] P. Di Pietro, OrtolaniM, LimajO, A. Di Gaspare, GilibertiV, GiorgianniF, BrahlekM, BansalN, KoiralaN, OhS, CalvaniP, LupiS, Observation of Dirac plasmons in a topological insulator, Nat Nano, 8 (2013) 556-560.
- [15] J.-Y. Ou, J.-K. So, G. Adamo, A. Sulaev, L. Wang, N.I. Zheludev, Ultraviolet and visible range plasmonics in the topological insulator Bi<sub>1.5</sub>Sb<sub>0.5</sub>Te<sub>1.8</sub>Se<sub>1.2</sub>, Nat Commun, 5 (2014).
- [16] Z. Yue, B. Cai, L. Wang, X. Wang, M. Gu, Intrinsically core-shell plasmonic dielectric nanostructures with ultrahigh refractive index, Science Advances, 2 (2016).
- [17] Z. Yue, G. Xue, J. Liu, Y. Wang, M. Gu, Nanometric holograms based on a topological insulator material, 8 (2017) 15354.

- [18] X. Zhang, J. Wang, S.-C. Zhang, Topological insulators for high-performance terahertz to infrared applications, *Physical Review B*, 82 (2010) 245107.
- [19] C.L. Kane, E.J. Mele, Quantum Spin Hall Effect in Graphene, *Physical Review Letters*, 95 (2005) 226801.
- [20] B.A. Bernevig, S.-C. Zhang, Quantum Spin Hall Effect, *Physical Review Letters*, 96 (2006) 106802.
- [21] M. König, S. Wiedmann, C. Brüne, A. Roth, H. Buhmann, L.W. Molenkamp, X.-L. Qi, S.-C. Zhang, Quantum Spin Hall Insulator State in HgTe Quantum Wells, *Science*, 318 (2007) 766-770.
- [22] A. Roth, C. Brüne, H. Buhmann, L.W. Molenkamp, J. Maciejko, X.-L. Qi, S.-C. Zhang, Nonlocal Transport in the Quantum Spin Hall State, *Science*, 325 (2009) 294-297.
- [23] F. Reis, G. Li, L. Dudy, M. Bauernfeind, S. Glass, W. Hanke, R. Thomale, J. Schäfer, R. Claessen, Bismuthene on a SiC substrate: A candidate for a high-temperature quantum spin Hall material, *Science*, DOI 10.1126/science.aai8142(2017).
- [24] S. Wu, V. Fatemi, Q.D. Gibson, K. Watanabe, T. Taniguchi, R.J. Cava, P. Jarillo-Herrero, Observation of the quantum spin Hall effect up to 100 kelvin in a monolayer crystal, *Science*, 359 (2018) 76-79.
- [25] X.-L. Qi, T.L. Hughes, S.-C. Zhang, Topological field theory of time-reversal invariant insulators, *Physical Review B*, 78 (2008) 195424.
- [26] X.-L. Qi, R. Li, J. Zang, S.-C. Zhang, Inducing a Magnetic Monopole with Topological Surface States, *Science*, 323 (2009) 1184-1187.
- [27] X.-L. Qi, T.L. Hughes, S.-C. Zhang, Chiral topological superconductor from the quantum Hall state, *Physical Review B*, 82 (2010) 184516.
- [28] L. Fu, C.L. Kane, Superconducting Proximity Effect and Majorana Fermions at the Surface of a Topological Insulator, *Physical Review Letters*, 100 (2008) 096407.
- [29] V. Mourik, K. Zuo, S.M. Frolov, S.R. Plissard, E.P.A.M. Bakkers, L.P. Kouwenhoven, Signatures of Majorana Fermions in Hybrid Superconductor-Semiconductor Nanowire Devices, *Science*, 336 (2012) 1003-1007.
- [30] A. Das, Y. Ronen, Y. Most, Y. Oreg, M. Heiblum, H. Shtrikman, Zero-bias peaks and splitting in an Al-InAs nanowire topological superconductor as a signature of Majorana fermions, *Nat Phys*, 8 (2012) 887-895.
- [31] L.P. Rokhinson, X. Liu, J.K. Furdyna, The fractional a.c. Josephson effect in a semiconductor-superconductor nanowire as a signature of Majorana particles, *Nat Phys*, 8 (2012) 795-799.

- [32] A. Stern, N.H. Lindner, Topological Quantum Computation—From Basic Concepts to First Experiments, *Science*, 339 (2013) 1179-1184.
- [33] Q.L. He, L. Pan, A.L. Stern, E.C. Burks, X. Che, G. Yin, J. Wang, B. Lian, Q. Zhou, E.S. Choi, K. Murata, X. Kou, Z. Chen, T. Nie, Q. Shao, Y. Fan, S.-C. Zhang, K. Liu, J. Xia, K.L. Wang, Chiral Majorana fermion modes in a quantum anomalous Hall insulator–superconductor structure, *Science*, 357 (2017) 294-299.
- [34] S.J. Callori, S. Hu, J. Bertinshaw, Z.J. Yue, S. Danilkin, X.L. Wang, V. Nagarajan, F. Klöse, J. Seidel, C. Ulrich, Strain-induced magnetic phase transition in SrCoO<sub>3-δ</sub> thin films, *Physical Review B*, 91 (2015) 140405.
- [35] S. Hu, Z. Yue, J.S. Lim, S.J. Callori, J. Bertinshaw, A. Ikeda-Ohno, T. Ohkochi, C.H. Yang, X. Wang, C. Ulrich, J. Seidel, Growth and Properties of Fully Strained SrCoO<sub>x</sub> ( $x \approx 2.8$ ) Thin Films on DyScO<sub>3</sub>, *Advanced Materials Interfaces*, 2 (2015) 1500012-n/a.
- [36] Z.J. Yue, D.H. Seo, K. Ostrikov, X.L. Wang, Defects induced ferromagnetism in plasma-enabled graphene nanopetals, *Applied Physics Letters*, 104 (2014) 092417.
- [37] D. Seo, Z. Yue, X. Wang, I. Levchenko, S. Kumar, S. Dou, K. Ostrikov, Tuning of magnetization in vertical graphenes by plasma-enabled chemical conversion of organic precursors with different oxygen content, *Chemical Communications*, 49 (2013) 11635-11637.
- [38] R. Yu, W. Zhang, H.-J. Zhang, S.-C. Zhang, X. Dai, Z. Fang, Quantized Anomalous Hall Effect in Magnetic Topological Insulators, *Science*, 329 (2010) 61-64.
- [39] C.-Z. Chang, J. Zhang, X. Feng, J. Shen, Z. Zhang, M. Guo, K. Li, Y. Ou, P. Wei, L.-L. Wang, Z.-Q. Ji, Y. Feng, S. Ji, X. Chen, J. Jia, X. Dai, Z. Fang, S.-C. Zhang, K. He, Y. Wang, L. Lu, X.-C. Ma, Q.-K. Xue, Experimental Observation of the Quantum Anomalous Hall Effect in a Magnetic Topological Insulator, *Science*, 340 (2013) 167-170.
- [40] X.L. Wang, Proposal for a New Class of Materials: Spin Gapless Semiconductors, *Physical Review Letters*, 100 (2008) 156404.
- [41] X.-L. Wang, S.X. Dou, C. Zhang, Zero-gap materials for future spintronics, electronics and optics, *Npg Asia Materials*, 2 (2010) 31.
- [42] X.-L. Wang, Dirac spin-gapless semiconductors: promising platforms for massless and dissipationless spintronics and new (quantum) anomalous spin Hall effects, *National Science Review*, 4 (2017) 252-257.
- [43] C.-X. Liu, S.-C. Zhang, X.-L. Qi, The Quantum Anomalous Hall Effect: Theory and Experiment, *Annual Review of Condensed Matter Physics*, 7 (2016) 301-321.

- [44] Z. Yue, X. Wang, D. Wang, J. Wang, D. Culcer, S. Dou, Crossover of magnetoresistance from fourfold to twofold symmetry in SmB<sub>6</sub> single crystal, a topological Kondo insulator, *Journal of the Physical Society of Japan*, 84 (2015) 044717.
- [45] Z. Yue, C. Zhu, S. Dou, X. Wang, Observation of field-induced polarization of valleys in p-type Sb<sub>2</sub>Te<sub>3</sub> single crystals, *Physical Review B*, 86 (2012) 195120.
- [46] Z.J. Yue, X.L. Wang, S.S. Yan, Semimetal-semiconductor transition and giant linear magnetoresistances in three-dimensional Dirac semimetal Bi<sub>0.96</sub>Sb<sub>0.04</sub> single crystals, *Applied Physics Letters*, 107 (2015) 112101.
- [47] Z. Yue, I. Levchenko, S. Kumar, D. Seo, X. Wang, S. Dou, K. Ostrikov, Large networks of vertical multi-layer graphenes with morphology-tunable magnetoresistance, *Nanoscale*, 5 (2013) 9283-9288.
- [48] Z.J. Yue, X.L. Wang, S.X. Dou, Angular-dependences of giant in-plane and interlayer magnetoresistances in Bi<sub>2</sub>Te<sub>3</sub> bulk single crystals, *Applied Physics Letters*, 101 (2012) 152107.
- [49] Z. Yue, X. Wang, S. Dou, Giant interlayer magnetoresistances and strong anisotropy in p-type Sb<sub>2</sub>Te<sub>3</sub> single crystals, *Integrated Ferroelectrics*, 140 (2012) 155-160.
- [50] Z. Yue, X. Wang, S.-S. Yan, Semimetal-semiconductor transition and giant linear magnetoresistances in three-dimensional Dirac semimetal Bi<sub>0.96</sub>Sb<sub>0.04</sub> single crystals, *Applied Physics Letters*, 107 (2015) 112101.
- [51] F.-X. Xiang, X.-L. Wang, M. Veldhorst, S.-X. Dou, M.S. Fuhrer, Observation of topological transition of Fermi surface from a spindle torus to a torus in bulk Rashba spin-split BiTeCl, *Physical Review B*, 92 (2015) 035123.
- [52] Z. Yue, X. Wang, Y. Du, S. Mahboobeh, F.F. Yun, Z. Cheng, S. Dou, Giant and anisotropic magnetoresistances in p-type Bi-doped Sb<sub>2</sub>Te<sub>3</sub> bulk single crystals, *EPL (Europhysics Letters)*, 100 (2012) 17014.
- [53] B. Xia, P. Ren, A. Sulaev, P. Liu, S.-Q. Shen, L. Wang, Indications of surface-dominated transport in single crystalline nanoflake devices of topological insulator Bi<sub>1.5</sub>Sb<sub>0.5</sub>Te<sub>1.8</sub>Se<sub>1.2</sub>, *Physical Review B*, 87 (2013) 085442.
- [54] A. Sulaev, M. Zeng, S.-Q. Shen, S.K. Cho, W.G. Zhu, Y.P. Feng, S.V. Eremeev, Y. Kawazoe, L. Shen, L. Wang, Electrically Tunable In-Plane Anisotropic Magnetoresistance in Topological Insulator BiSbTeSe<sub>2</sub> Nanodevices, *Nano Letters*, 15 (2015) 2061-2066.
- [55] L. Bao, L. He, N. Meyer, X. Kou, P. Zhang, Z.-g. Chen, A.V. Fedorov, J. Zou, T.M. Riedemann, T.A. Lograsso, K.L. Wang, G. Tuttle, F. Xiu, Weak Anti-localization and

- Quantum Oscillations of Surface States in Topological Insulator  $\text{Bi}_2\text{Se}_2\text{Te}$ , *Sci. Rep.*, 2 (2012).
- [56] D.-X. Qu, Y.S. Hor, J. Xiong, R.J. Cava, N.P. Ong, Quantum Oscillations and Hall Anomaly of Surface States in the Topological Insulator  $\text{Bi}_2\text{Te}_3$ , *Science*, 329 (2010) 821-824.
- [57] A.A. Taskin, Y. Ando, Quantum oscillations in a topological insulator  $\text{Bi}_{1-x}\text{Sb}_x$ , *Physical Review B*, 80 (2009) 085303.
- [58] H. He, B. Li, H. Liu, X. Guo, Z. Wang, M. Xie, J. Wang, High-field linear magnetoresistance in topological insulator  $\text{Bi}_2\text{Se}_3$  thin films, *Applied Physics Letters*, 100 (2012) 032105.
- [59] H. Tang, D. Liang, R.L.J. Qiu, X.P.A. Gao, Two-Dimensional Transport-Induced Linear Magneto-Resistance in Topological Insulator  $\text{Bi}_2\text{Se}_3$  Nanoribbons, *ACS Nano*, 5 (2011) 7510-7516.
- [60] S.-P. Chiu, J.-J. Lin, Weak antilocalization in topological insulator  $\text{Bi}_2\text{Te}_3$  microflakes, *Physical Review B*, 87 (2013) 035122.
- [61] X. Wang, Y. Du, S. Dou, C. Zhang, Room Temperature Giant and Linear Magnetoresistance in Topological Insulator  $\text{Bi}_2\text{Te}_3$  Nanosheets, *Physical Review Letters*, 108 (2012) 266806.
- [62] A.A. Abrikosov, Quantum magnetoresistance, *Physical Review B*, 58 (1998) 2788-2794.
- [63] A.A. Abrikosov, Quantum magnetoresistance of layered semimetals, *Physical Review B*, 60 (1999) 4231-4234.
- [64] H.-Z. Lu, J. Shi, S.-Q. Shen, Competition between Weak Localization and Antilocalization in Topological Surface States, *Physical Review Letters*, 107 (2011) 076801.
- [65] J. Chen, H.J. Qin, F. Yang, J. Liu, T. Guan, F.M. Qu, G.H. Zhang, J.R. Shi, X.C. Xie, C.L. Yang, K.H. Wu, Y.Q. Li, L. Lu, Gate-Voltage Control of Chemical Potential and Weak Antilocalization in  $\text{Bi}_2\text{Se}_3$ , *Physical Review Letters*, 105 (2010) 176602.
- [66] H.-T. He, G. Wang, T. Zhang, I.-K. Sou, G.K.L. Wong, J.-N. Wang, H.-Z. Lu, S.-Q. Shen, F.-C. Zhang, Impurity Effect on Weak Antilocalization in the Topological Insulator  $\text{Bi}_2\text{Te}_3$ , *Physical Review Letters*, 106 (2011) 166805.
- [67] M. Liu, J. Zhang, C.-Z. Chang, Z. Zhang, X. Feng, K. Li, K. He, L.-l. Wang, X. Chen, X. Dai, Z. Fang, Q.-K. Xue, X. Ma, Y. Wang, Crossover between Weak Antilocalization and Weak Localization in a Magnetically Doped Topological Insulator, *Physical Review Letters*, 108 (2012) 036805.



- [68] M. Lang, L. He, X. Kou, P. Upadhyaya, Y. Fan, H. Chu, Y. Jiang, J.H. Bardarson, W. Jiang, E.S. Choi, Y. Wang, N.-C. Yeh, J. Moore, K.L. Wang, Competing Weak Localization and Weak Antilocalization in Ultrathin Topological Insulators, *Nano Letters*, 13 (2012) 48-53.
- [69] H.-Z. Lu, S.-Q. Shen, Weak localization of bulk channels in topological insulator thin films, *Physical Review B*, 84 (2011) 125138.
- [70] J. Xiong, Y. Luo, Y. Khoo, S. Jia, R.J. Cava, N.P. Ong, High-field Shubnikov–de Haas oscillations in the topological insulator  $\text{Bi}_2\text{Te}_2\text{Se}$ , *Physical Review B*, 86 (2012) 045314.
- [71] L.L. Chang, H. Sakaki, C.A. Chang, L. Esaki, Shubnikov—de Haas Oscillations in a Semiconductor Superlattice, *Physical Review Letters*, 38 (1977) 1489-1493.
- [72] S. Ishiwata, Y. Shiomi, J.S. Lee, M.S. Bahramy, T. Suzuki, M. Uchida, R. Arita, Y. Taguchi, Y. Tokura, Extremely high electron mobility in a phonon-glass semimetal, *Nat Mater*, 12 (2013) 512-517.
- [73] W. Wang, Y. Du, G. Xu, X. Zhang, E. Liu, Z. Liu, Y. Shi, J. Chen, G. Wu, X.-x. Zhang, Large Linear Magnetoresistance and Shubnikov-de Hass Oscillations in Single Crystals of  $\text{YPdBi}$  Heusler Topological Insulators, *Sci. Rep.*, 3 (2013).
- [74] M. Tian, W. Ning, Z. Qu, H. Du, J. Wang, Y. Zhang, Dual evidence of surface Dirac states in thin cylindrical topological insulator  $\text{Bi}_2\text{Te}_3$  nanowires, *Sci. Rep.*, 3 (2013).
- [75] E. Goi, Z. Yue, B.P. Cumming, M. Gu, Observation of Type I Photonic Weyl Points in Optical Frequencies, *Laser & Photonics Reviews*, 12 (2018) 1700271-n/a.
- [76] Y. Zengji, C. Qinjun, S. Amit, W. Xiaolin, G. Min, Photo-oxidation-modulated refractive index in  $\text{Bi}_2\text{Te}_3$  thin films, *Materials Research Express*, 4 (2017) 126403.
- [77] E. Goi, Z. Yue, B.P. Cumming, M. Gu, Two-photon fabrication of type I optical Weyl points in photonic crystals, *Frontiers in Optics 2017*, Optical Society of America, Washington, D.C., 2017, pp. FW6C.5.
- [78] Z. Yue, M. Gu, Resonant cavity-enhanced holographic imaging in ultrathin topological insulator films, *Frontiers in Optics*, Optical Society of America, 2016, pp. FTu3F. 1.
- [79] H. Peng, W. Dang, J. Cao, Y. Chen, D. Wu, W. Zheng, H. Li, Z.-X. Shen, Z. Liu, Topological insulator nanostructures for near-infrared transparent flexible electrodes, *Nat Chem*, 4 (2012) 281-286.
- [80] L. Ge, T. Zhan, D. Han, X. Liu, J. Zi, Unusual electromagnetic scattering by cylinders of topological insulator, *Opt. Express*, 22 (2014) 30833-30842.
- [81] S.A. Maier, *Plasmonics: fundamentals and applications*, Springer Science & Business Media 2007.

- [82] Z. Fang, X. Zhu, Plasmonics in nanostructures, *Advanced Materials*, 25 (2013) 3840-3856.
- [83] Q. Zhang, X. Li, M.M. Hossain, Y. Xue, J. Zhang, J. Song, J. Liu, M.D. Turner, S. Fan, Q. Bao, M. Gu, Graphene surface plasmons at the near-infrared optical regime, 4 (2014) 6559.
- [84] S. Sim, H. Jang, N. Koirala, M. Brahlek, J. Moon, J.H. Sung, J. Park, S. Cha, S. Oh, M.-H. Jo, J.-H. Ahn, H. Choi, Ultra-high modulation depth exceeding 2,400% in optically controlled topological surface plasmons, *Nature Communications*, 6 (2015) 8814.
- [85] M. Zhao, J. Zhang, N. Gao, P. Song, M. Bosman, B. Peng, B. Sun, C.-W. Qiu, Q.-H. Xu, Q. Bao, K.P. Loh, Actively Tunable Visible Surface Plasmons in  $\text{Bi}_2\text{Te}_3$  and their Energy-Harvesting Applications, *Advanced Materials*, 28 (2016) 3138-3144.
- [86] M. Zhao, M. Bosman, M. Danesh, M. Zeng, P. Song, Y. Darma, A. Rusydi, H. Lin, C.-W. Qiu, K.P. Loh, Visible Surface Plasmon Modes in Single  $\text{Bi}_2\text{Te}_3$  Nanoplate, *Nano Letters*, 15 (2015) 8331-8335.
- [87] J. Yuan, W. Ma, L. Zhang, Y. Lu, M. Zhao, H. Guo, J. Zhao, W. Yu, Y. Zhang, K. Zhang, H.Y. Hoh, X. Li, K.P. Loh, S. Li, C.-W. Qiu, Q. Bao, Infrared Nanoimaging Reveals the Surface Metallic Plasmons in Topological Insulator, *ACS Photonics*, DOI 10.1021/acsp Photonics.7b00568(2017).
- [88] J. Yin, H.N.S. Krishnamoorthy, G. Adamo, A.M. Dubrovkin, Y. Chong, N.I. Zheludev, C. Soci, Plasmonics of topological insulators at optical frequencies, *Npg Asia Materials*, 9 (2017) e425.
- [89] A.M. Dubrovkin, G. Adamo, J. Yin, L. Wang, C. Soci, Q.J. Wang, N.I. Zheludev, Visible Range Plasmonic Modes on Topological Insulator Nanostructures, *Advanced Optical Materials*, 5 (2017) 1600768-n/a.
- [90] J.W. McIver, HsiehD, SteinbergH, P. Jarillo Herrero, GedikN, Control over topological insulator photocurrents with light polarization, *Nat Nano*, 7 (2012) 96-100.
- [91] S. Chen, C. Zhao, Y. Li, H. Huang, S. Lu, H. Zhang, S. Wen, Broadband optical and microwave nonlinear response in topological insulator, *Opt. Mater. Express*, 4 (2014) 587-596.
- [92] F. Giorgianni, E. Chiadroni, A. Rovere, M. Cestelli-Guidi, A. Perucchi, M. Bellaveglia, M. Castellano, D. Di Giovenale, G. Di Pirro, M. Ferrario, R. Pompili, C. Vaccarezza, F. Villa, A. Cianchi, A. Mostacci, M. Petrarca, M. Brahlek, N. Koirala, S. Oh, S. Lupi, Strong nonlinear terahertz response induced by Dirac surface states in  $\text{Bi}_2\text{Se}_3$  topological insulator, 7 (2016) 11421.

- [93] S. Lu, C. Zhao, Y. Zou, S. Chen, Y. Chen, Y. Li, H. Zhang, S. Wen, D. Tang, Third order nonlinear optical property of Bi<sub>2</sub>Se<sub>3</sub>, *Opt. Express*, 21 (2013) 2072-2082.
- [94] Z. Yue, H. Ren, M. Gu, Ultrathin double-focusing topological insulator lens, 2017 Conference on Lasers and Electro-Optics Pacific Rim (CLEO-PR), 2017, pp. 1-1.
- [95] E. Goi, Z.J. Yue, B.P. Cumming, M. Gu, Complete bandgap in three-dimensional chiral gyroid photonic crystals for topological photonics, *Lasers and Electro-Optics (CLEO)*, 2016 Conference on, IEEE, 2016, pp. 1-2.
- [96] Z.J. Yue, K. Zhao, S.Q. Zhao, Z.Q. Lu, X.M. Li, H. Ni, A.J. Wang, Thickness-dependent photovoltaic effects in miscut Nb-doped SrTiO<sub>3</sub> single crystals, *Journal of Physics D: Applied Physics*, 43 (2009) 015104.
- [97] X. Li, K. Zhao, H. Ni, S. Zhao, W. Xiang, Z. Lu, Z. Yue, F. Wang, Y.-C. Kong, H. Wong, Voltage tunable photodetecting properties of La<sub>0.4</sub>Ca<sub>0.6</sub>MnO<sub>3</sub> films grown on miscut LaSrAlO<sub>4</sub> substrates, *Applied Physics Letters*, 97 (2010) 044104.
- [98] Z. Yue, K. Zhao, H. Ni, S. Zhao, Y. Kong, H. Wong, A. Wang, Photo-induced magnetoresistance enhancement in manganite heterojunction at room temperature, *Journal of Physics D: Applied Physics*, 44 (2011) 095103.
- [99] H. Ni, Z. Yue, K. Zhao, W. Xiang, S. Zhao, A. Wang, Y.-C. Kong, H.-K. Wong, Magnetical and electrical tuning of transient photovoltaic effects in manganite-based heterojunctions, *Opt. Express*, 20 (2012) A406-A411.
- [100] A. Sharma, B. Bhattacharyya, A.K. Srivastava, T.D. Senguttuvan, S. Husale, High performance broadband photodetector using fabricated nanowires of bismuth selenide, 6 (2016) 19138.
- [101] H. Plank, S.N. Danilov, V.V. Bel'kov, V.A. Shalygin, J. Kampmeier, M. Lanius, G. Mussler, D. Grützmacher, S.D. Ganichev, Opto-electronic characterization of three dimensional topological insulators, *Journal of Applied Physics*, 120 (2016) 165301.
- [102] K. Zheng, L.-B. Luo, T.-F. Zhang, Y.-H. Liu, Y.-Q. Yu, R. Lu, H.-L. Qiu, Z.-J. Li, J.C. Andrew Huang, Optoelectronic characteristics of a near infrared light photodetector based on a topological insulator Sb<sub>2</sub>Te<sub>3</sub> film, *Journal of Materials Chemistry C*, 3 (2015) 9154-9160.
- [103] C. Zhao, H. Zhang, X. Qi, Y. Chen, Z. Wang, S. Wen, D. Tang, Ultra-short pulse generation by a topological insulator based saturable absorber, *Applied Physics Letters*, 101 (2012) 211106.
- [104] J. Li, H. Luo, L. Wang, C. Zhao, H. Zhang, H. Li, Y. Liu, 3um mid-infrared pulse generation using topological insulator as the saturable absorber, *Opt. Lett.*, 40 (2015) 3659-3662.

- [105] J. Lee, J. Koo, Y.M. Jhon, J.H. Lee, A femtosecond pulse erbium fiber laser incorporating a saturable absorber based on bulk-structured  $\text{Bi}_2\text{Te}_3$  topological insulator, *Opt. Express*, 22 (2014) 6165-6173.
- [106] Y. Chen, C. Zhao, S. Chen, J. Du, P. Tang, G. Jiang, H. Zhang, S. Wen, D. Tang, Large Energy, Wavelength Widely Tunable, Topological Insulator Q-Switched Erbium-Doped Fiber Laser, *IEEE Journal of Selected Topics in Quantum Electronics*, 20 (2014) 315-322.
- [107] Z.-C. Luo, M. Liu, H. Liu, X.-W. Zheng, A.-P. Luo, C.-J. Zhao, H. Zhang, S.-C. Wen, W.-C. Xu, GHz passively harmonic mode-locked fiber laser by a microfiber-based topological insulator saturable absorber, *Opt. Lett.*, 38 (2013) 5212-5215.
- [108] Y.-H. Lin, S.-F. Lin, Y.-C. Chi, C.-L. Wu, C.-H. Cheng, W.-H. Tseng, J.-H. He, C.-I. Wu, C.-K. Lee, G.-R. Lin, Using n- and p-Type  $\text{Bi}_2\text{Te}_3$  Topological Insulator Nanoparticles To Enable Controlled Femtosecond Mode-Locking of Fiber Lasers, *ACS Photonics*, 2 (2015) 481-490.
- [109] J.-L. Xu, Y.-J. Sun, J.-L. He, Y. Wang, Z.-J. Zhu, Z.-Y. You, J.-F. Li, M.M.C. Chou, C.-K. Lee, C.-Y. Tu, Ultrasensitive nonlinear absorption response of large-size topological insulator and application in low-threshold bulk pulsed lasers, 5 (2015) 14856.
- [110] H. Yu, H. Zhang, Y. Wang, C. Zhao, B. Wang, S. Wen, H. Zhang, J. Wang, Topological insulator as an optical modulator for pulsed solid-state lasers, *Laser & Photonics Reviews*, 7 (2013) L77-L83.
- [111] C. Zhao, Y. Zou, Y. Chen, Z. Wang, S. Lu, H. Zhang, S. Wen, D. Tang, Wavelength-tunable picosecond soliton fiber laser with Topological Insulator:  $\text{Bi}_2\text{Se}_3$  as a mode locker, *Opt. Express*, 20 (2012) 27888-27895.
- [112] H. Liu, X.-W. Zheng, M. Liu, N. Zhao, A.-P. Luo, Z.-C. Luo, W.-C. Xu, H. Zhang, C.-J. Zhao, S.-C. Wen, Femtosecond pulse generation from a topological insulator mode-locked fiber laser, *Opt. Express*, 22 (2014) 6868-6873.
- [113] Z. Dou, Y. Song, J. Tian, J. Liu, Z. Yu, X. Fang, Mode-locked ytterbium-doped fiber laser based on topological insulator:  $\text{Bi}_2\text{Se}_3$ , *Opt. Express*, 22 (2014) 24055-24061.
- [114] Z. Yu, Y. Song, J. Tian, Z. Dou, H. Guoyu, K. Li, H. Li, X. Zhang, High-repetition-rate Q-switched fiber laser with high quality topological insulator  $\text{Bi}_2\text{Se}_3$  film, *Opt. Express*, 22 (2014) 11508-11515.
- [115] L. Gao, W. Huang, J.D. Zhang, T. Zhu, H. Zhang, C.J. Zhao, W. Zhang, H. Zhang, Q-switched mode-locked erbium-doped fiber laser based on topological insulator  $\text{Bi}_2\text{Se}_3$  deposited fiber taper, *Applied Optics*, 53 (2014) 5117-5122.